Ionic liquid based printable materials for thermochromic and thermoresistive applications

Liliana C. Fernandes[1], Daniela M. Correia[2,3], Clara García-Astrain[1], Nelson Pereira[3], Mohammad Tariq[4], José M.S.S. Esperança[4], Senentxu Lanceros-Méndez[1,5]**

[1]BCMaterials, Basque Center for Materials, Applications and Nanostructures, UPV/EHU Science Park, 48940 Leioa, Spain

[2] Departamento de Química e CQ-VR, Universidade de Trás-os-Montes e Alto Douro, 5001-801 Vila Real, Portugal

[3]Centro de Física, Campus de Gualtar, Universidade do Minho, 4710-057 Braga, Portugal

[4]LAQV, REQUIMTE, Departamento de Química, Faculdade de Ciências e Tecnologia, Universidade Nova de Lisboa, 2829-516 Caparica, Portugal

[5]Ikerbasque, Basque Foundation for Science, 48013 Bilbao, Spain

*Corresponding author email address:
senentxu.lanceros@bcmaterials.net; dcorreia@utad.pt

KEYWORDS: $[Bmim]_2[NiCl_4]$, electroactive materials, ionic liquids, PVDF, smart materials, thermochromic materials

Abstract: Smart materials exhibiting thermochromic and themoresistive properties based on the electroactive polymer poly(vinylidene) (PVDF) and the ionic liquid (IL) bis(1-butyl-3-methylimidazolium) tetrachloronickelate ($[Bmim]_2[NiCl_4]$) have been developed with different contents of $[Bmim]_2[NiCl_4]$ (10, 20 and 40 wt. %) within the polymer matrix. The morphology of the composites is studied and the thermochromic and thermoresistive properties evaluated. Independently of the IL content, PVDF/$[Bmim]_2[NiCl_4]$ composites present a porous morphology and thermochromic response, revealed by the composites color change from transparent to a dark blue, and attributed to the tetrahedral complex $NiCl_4^{2-}$ formed after a dehydration process. Further, the electrical conductivity increases with increasing IL content and decreases with increasing temperature. It is also shown that the incorporation of the IL into the PVDF matrix leads to an increase in the electroactive β phase and a decrease of the degree of the crystallinity and thermal stability with increasing $[Bmim]_2[NiCl_4]$ content. The printability and applicability of the developed materials as sensors is demonstrated.

Introduction

Ionic liquids (ILs) are defined as salts entirely composed of ions with melting points below 100 ºC [1-2]. The increasing scientific and technological interest in ILs is mainly due to their tuneable properties, including high ionic conductivity, negligible vapor pressure, thermal, mechanical, chemical and electrochemical stability, including a wide liquid range [3-6]. The interest in ILs also relies in representing a greener alternative to solubilize organic, inorganic and polymeric materials replacing the traditional volatile organic solvents and traditional electrolytes in several processes [5].

ILs have emerged as relevant materials for the development of smart materials with new functionalities and applicability [7]. These materials are characterized by their ability to respond in a controlled manner to an external stimulus such as temperature, pH, magnetic and electric fields, among others, by changing their intrinsic properties, adapting to the environment conditions [7-8]. Depending on the cation and/or anion nature, it is possible to design and tune a high number of ILs with characteristics and functionalities relevant for the development of smart responsive and sensitive materials, including photoresponsive, pH-sensitive, electrochromic and thermochromic, among others [5, 7].

Thermochromic materials have been gaining increasing attention due to their ability to change color as a function of temperature, revealed by the gradual color change over a wide range of temperature as a result of the changes in the widths of the absorption bands [9]. The thermochromic behavior is exhibited by many transition metal complexes, such as nickel, copper and halide complexes [10], occurring the phenomena upon the interaction of the transition metal with an appropriate donor solvent due to the energy alternation of the d-d transitions and configuration changes [11-12]. Such phenomenon, characterized by a reversible colour change, takes place in response to a temperature variation either by heating or cooling

[11]. Thermochromic systems can be applied in several areas including energy [13-14], flexible electronics[15-16], textile industry [17-18] or smart food packaging [19], among others.

The development of materials combining ILs and polymers have been studied for several applications offering many advantages over the traditional materials including the high versatility and high potential building blocks [5]. Furthermore, the incorporation of ILs by chemical functionalization or ion-exchange metathesis of the ionic compounds into the polymer matrix leads obtaining ionic materials with new functionalities, combining the key features of the polymer and the characteristics of the ILs [5, 7].

Efforts have been also carried out in the development of IL-based materials combining electroactive polymers and ILs [20-22]. Due to its piezoelectric properties, poly(vinylidene fluoride), P(VDF), has been studied as a polymer matrix for the development of multifunctional materials [23-24]. PVDF is a semi-crystalline polymer with high ionic conductivity, dielectric constant, polarity and electroactive response, including piezo-, pyro-, and ferroelectric properties [25]. Although it presents four known crystalline phases, being the β phase the main responsible for its piezoelectric properties [25]. Developed IL-PVDF based materials find applicability in several areas such as sensors and actuators [26], energy generation and storage [27-28] or biomedicine [29], among others.

Few studies report on the thermochromic effect of polymer materials with incorporated ILs. PVDF with thermochromic ILs 1-(3-hydroxypropyl)-3-methylimidazolium tetrafluoroboride ($[C_3OHmim][BF_4]$) and di-(1-butyl-3-methylimidazolium) tetrachloronickelate ($[Bmim]_2[NiCl_4]$) were successfully prepared into stable solar-thermochromic composite films [30]. Also novel non-aqueous thermochromic systems based on PVDF and Ni (II)-deep eutectic solvent (DES) were developed for high performance thermochromic materials for the facile fabrications from DESs [21]. However, to the best of our knowledge no studies reports the effect of the integration of bulk $[Bmim]_2[NiCl_4]$ into the PVDF matrix, on the influence of IL concentration within the polymer matrix and into the electrochromic properties. Furthermore,

no reports exist on the influence of this IL into the physico-chemical, thermal and electrical properties of the composites.

In this work, a new reversible thermochromic and thermoresistive material based on PVDF/$[Bmim]_2[NiCl_4]$ was developed by solvent casting, showing also its applicability by printing technologies. The thermochromic, physico-chemical, electrical and thermal properties were evaluated at different IL concentrations and temperatures.

Experimental Section

Materials

The polymer PVDF (6010) (300 000-330 000 Da) was purchased from Solvay. The IL $[Bmim]_2[NiCl_4]$ (99 % purity) was synthesized as reported in [31-32]. The solvent N, N-dimethylformamide (DMF) (99.5 % purity) was purchased from Merck.

Composite processing

The preparation of the $[Bmim]_2[NiCl_4]$/PVDF composites were performed by solvent casting method, following the general guidelines presented in reference [32]. Different contents of IL (10, 20 and 40% wt.) were firstly dispersed into the DMF solvent to obtain a homogeneous solution. Then, PVDF was added in a ratio of 15/85 % wt. (PVDF/DMF) under mechanical agitation. After the complete polymer dissolution, the solution was spread into a glass at room temperature, followed by solvent evaporation at 210 ºC in an oven (P-Selecta) for 10 minutes (**Figure 1)**.

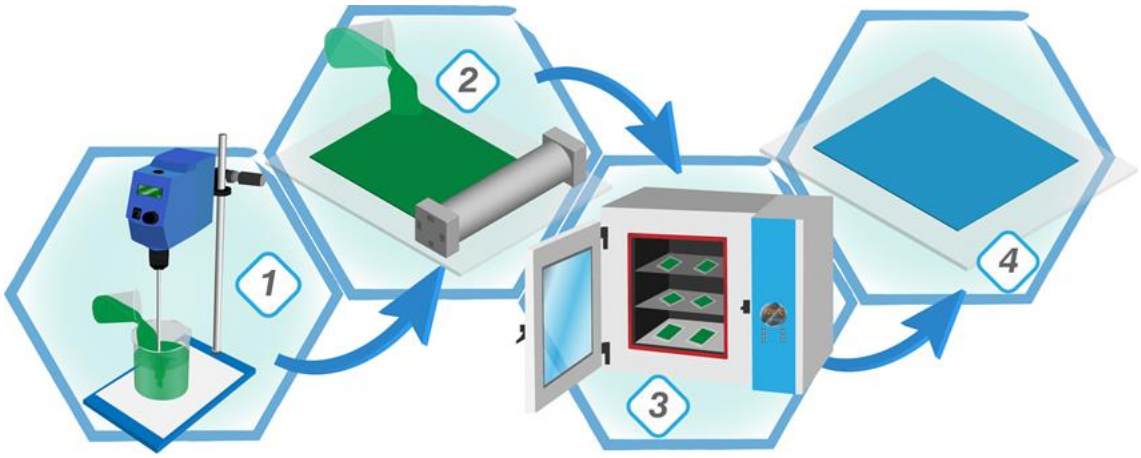

Figure 1. Schematic representation of the PVDF/IL composite films preparation:1- mechanical agitation, 2- solvent casting followed by spreading, 3- solvent evaporation, 4- obtained films.

Characterization

Morphology

The morphology of the IL/PVDF composites was evaluated using a scanning electron microscope (SEM, FEG-SEM Hitachi S4100) with an accelerating voltage of 10 kV. The samples were previously coated with a thin gold layer using sputter coating (Polaron, model SC502).

Physico-chemical characterization

The thermochromic effect was evaluated by Ultraviolet–visible spectroscopy (UV-VIS). UV-VIS spectra were collected on a Shimadzu UV-2550 with a temperature controller Shimadzu CPS-2440A. Spectra were recorded from 30 to 70 °C every 5 °C after 2-3 min stabilization period before each measurement. The temperature and relative humidity were measure by the Amprobe TR200-A, temperature and humidity data logger, in a vapor chamber with built-in temperature control. The humidity was introduced by an external humidifier.

The chemical properties of the composites were evaluated by Fourier transformed infrared (FTIR) performed in a JASCO FTIR 4100 set up in attenuated total reflectance (ATR) mode from 4000 to 600 cm^{-1}, using 64 scans with a resolution of 4 cm^{-1}. The β phase content was evaluated through the **Equation 1** [32]:

$$F(\beta) = \frac{A_\beta}{\left(K_\beta / K_\alpha\right)\left(A_\alpha + A_\beta\right)} \quad (1)$$

where A_α and A_β are the absorbances at 766 and 840 cm^{-1}, respectively and K_a and K_b are the absorption coefficients at the respective wavenumber (6.1×10^4 and 7.7×10^4 cm^2 mol^{-1}) .

X-Ray diffraction (XRD) as a function of temperature were performed with a Bruker D8 Advance diffractometer operating at 30 kV and 20 mA, equipped with a Cu tube (λ = 1.5418 Å), a Vantec-1 PSD detector, and an Anton Parr HTK2000 high-temperature furnace. The powder patterns were recorded in 2q steps of 0.033º in the 5 ≤2q ≤ 38 range, counting for 1 s per step (total time for each temperature 20 min). Data sets were recorded at different temperatures, 30, 40, 45, 50, 55, 60 and 70 ºC at 0.167 ºC s^{-1} during the heating and cooling rate.

The calorimetric analysis was performed by differential scanning calorimetry measurements (DSC) (Mettler Toledo DSC 821e apparatus) between 30 and 200 °C using a heating rate of 10 ºC min^{-1} under nitrogen purge. The degree of crystallinity (Xc) of each sample was evaluated using **Equation 2** [33]:

$$\chi = \frac{\Delta H}{x\Delta H_\alpha + y\Delta H_\beta} \quad (2)$$

where ΔH is the melting enthalpy of PVDF, ΔH_α and ΔH_β are the fusion enthalpies of α and β phase of PVDF (93.07 J g^{-1} and 103.4 J g^{-1} respectively) and x and y are α and β phase proportions of each sample.

The thermal degradation of the samples was evaluated using a thermogravimetric analysis (TGA) using a Perkin-Elmer TGA 4000 apparatus operating between 40 and 800 °C. For the measurements, the samples were placed in α-Al_2O_3 pans and a heating rate of 10 °C min^{-1} and a nitrogen atmosphere.

Electrical conductivity measurements

The electrical measurements of the composites were performed using a Keithley 6430 picoammeter/voltage source. For the measurements, the samples were prepared in the form of a parallel plate condenser with circular gold electrodes (5 mm diameter) deposited by magnetron sputtering with a Polaron Coater SC502 for good electric contact between sample and measurement equipment. The volume electrical conductivity was obtained at room temperature by the characteristic I-V curves. The current and voltage were measured. The conductivity (**σ**) was calculated attending to the geometrical factors of the samples according to the **Equation 3** [34]:

$$\sigma = {}^{1}/_{(RA/L)} \tag{3}$$

where RA/L is the electrical resistivity, R is the electrical resistance, L is the sample thickness and A is the area of the electrodes.

The variation of the electrical resistance of the samples composites was evaluated using an Agilent 34401A multimeter where the temperature was regulated with a Linkam THMSE 600, at a rate of 10 ºC min^{-1}, from room temperature to 200 ºC.

Results and discussion

Morphology and physico-chemical characterization

Figures 2a and 2b show the cross-section SEM images of neat PVDF and PVDF/$[Bmim]_2[NiCl_4]$ composites with 20 % wt. of $[Bmim]_2[NiCl_4]$. Similar results were obtained for the samples containing 10 and 40 % wt., being observed an increase of the number of pores with increasing IL content (**supplementary information S1**). Under the experimental conditions used in this work, after solvent evaporation, the neat PVDF film presents a non-porous homogenous surface (Figure 2a) [20]. The incorporation of $[Bmim]_2[NiCl_4]$ into the polymer matrix, originates a porous structure, as presented in **Figure 2b**, independently of the $[Bmim]_2[NiCl_4]$ content.

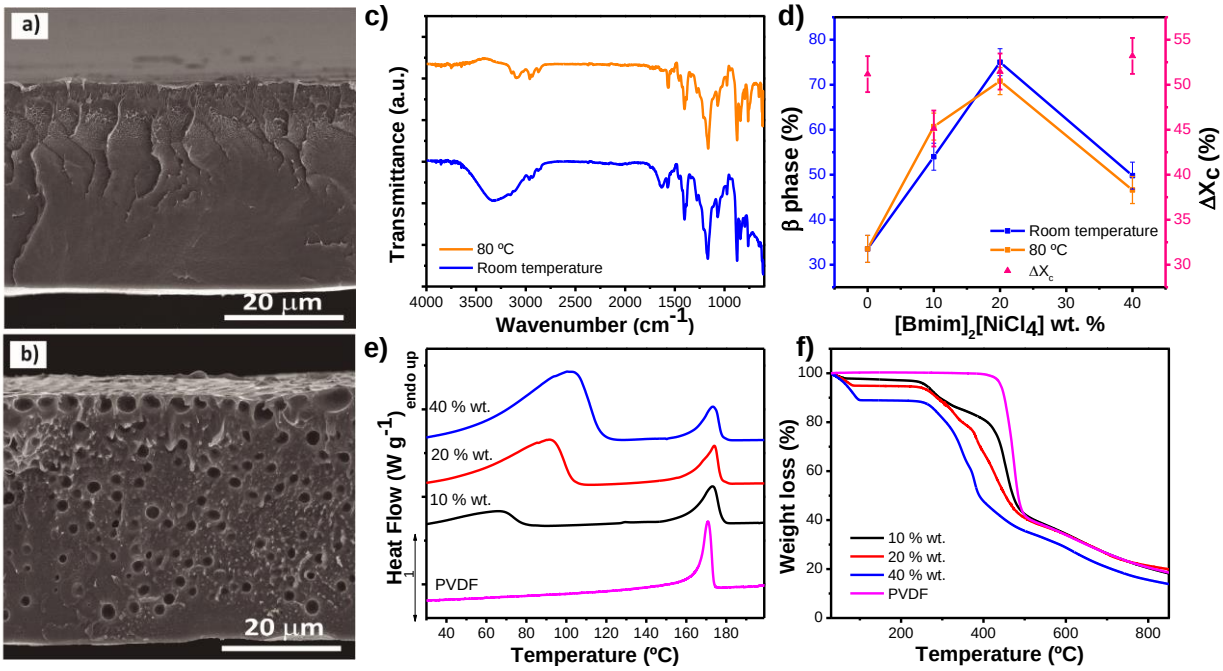

Figure 2. SEM cross-section images of PVDF (a) and PVDF/$[Bmim]_2[NiCl_4]$ with 20 % wt. (b). FTIR spectra of PVDF/$[Bmim]_2[NiCl_4]$ composites at room temperature and 80 °C for an IL content of 40 % wt. (c). β phase content and degree of crystallinity as a function of $[Bmim]_2[NiCl_4]$ content (d). DSC scans of the PVDF/$[Bmim]_2[NiCl_4]$ composites with

different IL contents (e) and thermogravimetric curves of the PVDF/$[Bmim]_2[NiCl_4]$ composites (f).

It is to notice that the observed porous structure fully results from the inclusion of the IL within the polymer matrix, as the processing conditions (melting and recrystallization of the polymer) should result in a compact structure [25]. The generation of the porous structure is attributed to the physical interaction between the IL with the aprotic and polar DMF solvent and a phase separation process of the polymer and IL+solvent systems[35]. During the DMF evaporation, due to the high dipolar moment of the DMF, there is a liquid -liquid phase separation of the polymer and the IL-solvent systems previous to the PVDF crystallization, the IL becoming encapsulated within the pores after DMF evaporation.

To study the influence of $[Bmim]_2[NiCl_4]$ addition in the electroactive phase of the PVDF, an infrared analysis at different temperatures was performed. FTIR spectra were recorded both at room temperature and at 80 °C (**Figure 2c**). Similar absorption bands are observed for all the composites containing different IL contents. According to the structure of the $[Bmim]^+$ cation, the bands at 2970, 2930 and 2870 cm^{-1} are attributed to the –C-H stretching vibration of $–CH_2$ and $–CH_3$ groups near the nitrogen atoms of the imidazolium ring [36]. The stretching vibration of the $–CH_2$ groups from the imidazolium ring were observed at 3140 and 3098 cm^{-1} whereas the skeleton vibrations range between 1600 and 1340 cm^{-1}. The C-N stretching vibration was observed at 1170 cm^{-1}. After heating the samples at 80 °C, it can be observed the absence of the two absorption bands at 3330 and 1637 cm^{-1} that correspond to the stretching and bending vibration modes of the H_2O molecules [37]. These results are particularly relevant as prove that, independently of the IL content into the polymer matrix, the change in color from transparent to blue of the film composite (see section 2.2) could be caused by the presence of water molecules into the coordination structure of the $[Bmim]_2[NiCl_4]$ followed by the release of the

coordinated water molecules when the polymer matrix composed by PVDF/$[Bmim]_2[NiCl_4]$ samples are heated at 80 ºC.

The absorption bands characteristic of the -CH_2-CF_2- PVDF chemical structure can be also observed in the FTIR-ATR spectra of **Figure 2c**. The vibrational modes at ~3022 and 2980 cm^{-1} are attributed to the stretching vibration of the asymmetric and symmetric vibration of the CH_2 groups. The wagging vibration of the CH_2 is characterized by the absorption band at 1403 cm^{-1}. The C-C stretching vibration is observed at 1185 cm^{-1}. The absorption bands at 855, 795 and 766 cm^{-1} are characteristics of the PVDF α phase. The electroactive β phase is detected at 840 cm^{-1}.

The β phase content was evaluated from **Equation 1**. As observed from **Figure 2d**, independently of the temperature, the IL content into the polymer matrix influences the β phase content of PVDF. There is an increase up to 20 % wt. of IL followed by a decrease as the IL content increases to 40% wt. Thus, the highest β phase values were obtained in the composite films with 20 % wt. of IL both at room temperature (70 %) and 80 ºC (75 %). These results indicate that the electrostatic interaction between the negative charge of the IL anion with the positive side of the PVDF dipoles (which promotes the orientation of the polymer chains in the all-trans chain conformation of the β-phase) decreases with an IL content into the polymer matrix higher than 20-30 %, due to competing interactions of the cation and the polymer chain for larger IL contents [38]. Thus, this electrostatic interaction promotes the crystallization of the polymer in the phase with the largest dielectric constant and electroactive response of PVDF [25]. It should also be noticed that generally the β phase content decreases as the solvent evaporation temperature increases and, in particular, that under the processing conditions used in this work (melting and recrystallization) PVDF crystallizes in the α-phase [25], showing that the crystallization of the electroactive β-phase is fully ascribed to the presence of the IL.

Figure 2e shows the DSC curves of the PVDF/$[Bmim]_2[NiCl_4]$, characterized by two endothermic peaks. The peak observed for all the PVDF/$[Bmim]_2[NiCl_4]$ composites between ~60 and 100 ºC is attributed to water desorption [39], increasing the endotherm peak area with increasing IL content into the polymer matrix due to its hygroscopic characteristics. The endothermic peak observed between 150-190 ºC is attributed to the melting of PVDF[25].

The evolution of the degree of crystallinity, ΔX_C, with increasing $[Bmim]_2[NiCl_4]$ content is presented in **Figure 2d**, showing just slight variations. Thus, the degree of crystallinity (evaluated trough **Equation 2**) ranges from 51 % for the neat PVDF to 55 % for the composite containing 40 % wt. IL content. For smaller amounts of IL, i.e. 10 % wt., a decrease of ΔX_C to 45 % is observed. This behavior is explained by the strong interactions of the $[Bmim]_2[NiCl_4]$ with the PVDF polymer chain, that for low IL concentrations acts just as a defect, decreasing the crystallinity. For higher IL contents, on the other hand, $[Bmim]_2[NiCl_4]$ provides more nucleation centers, affecting the polymer crystallization kinetics and leading to a larger number of smaller spherulites, but with a similar degree of crystallinity[38].

From the TGA curves presented in **Figure 2f** it is observed that the PVDF degradation occurs in a single step and that for all composites three degradation steps are present. The first degradation step is attributed to water loss, corroborating the presence of water into the samples at room temperature due to the hygroscopic characteristics of the IL. The small weight loss observed at ~250 ºC is associated to volatile impurities from the IL [32]. $[B_nmim]_2[NiCl_4]$ salts thermally decompose in several steps. The onset decomposition of imidazolium cations starts to occur at about 300 ºC with an end temperature of thermal decomposition at ~430ºC. With increasing temperature, the nickel chloride tends to reduce to $Ni+NiCl_2$ [32].

The degradation observed above 400 ºC is attributed to PVDF, with the major weight loss occurring about 420 ºC. During this step the scission of the carbon-hydrogen bonds starts to

occurs primarily, followed by the carbon-fluorine scission (high bond strength of 460 Kj mol^{-1})[40] . From the thermograms it is also observed a general decrease in the thermal stability of the samples with increasing $[Bmim]_2[NiCl_4]$ content, which is attributed to the interaction of the degradation products of the IL with the polymer matrix.

To evaluate possible variations in the crystalline conformation of the composite films with temperature, XRD analysis was performed at different temperatures between 30 and 70ºC. The heating and cooling results of the PVDF/$[Bmim]_2[NiCl_4]$ composites with 20 % wt. of IL are shown in **Figure 3**. Similar results were obtained for the samples containing 10 and 40 % wt. of $[Bmim]_2[NiCl_4]$.

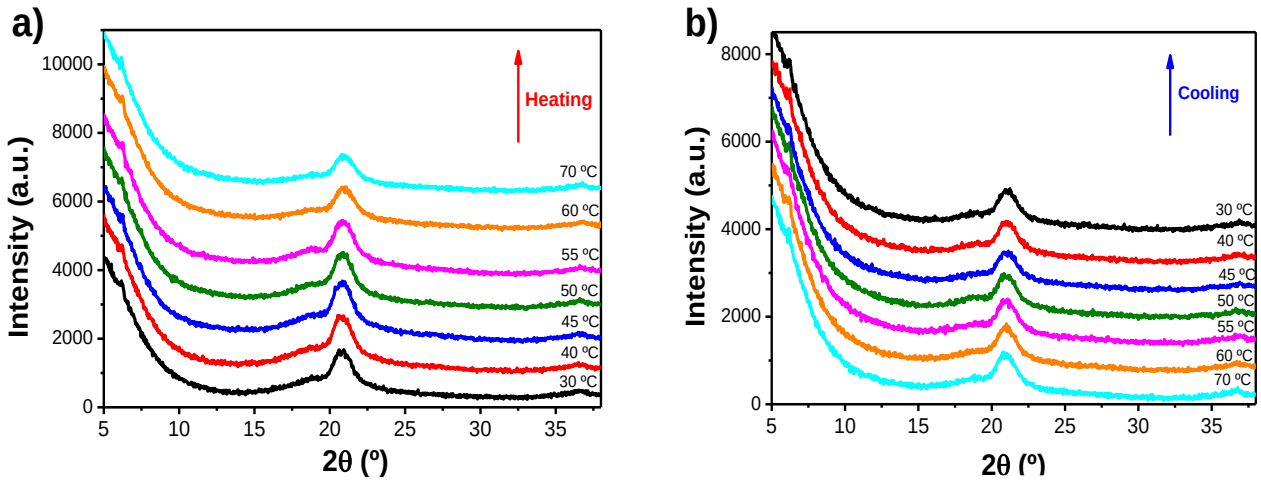

Figure 3. Temperature dependent X-Ray diffraction patterns for the composite with 20 % wt. of $[Bmim]_2[NiCl_4]$ content under a) heating and b) cooling.

Independently of the temperature, two peaks of diffraction at 2θ=6.0º and 2θ=20.88º are observed during the heating and the cooling of the samples. These diffraction peaks are assigned to the $[Bmim]_2[NiCl_4]$ and PVDF, respectively. The diffraction peak at 2θ=6.0º indicates the presence of a pseudocrystalline phase of the $[Bmim]_2[NiCl_4]$, thus proving the immobilization of the IL into the PVDF structure [30]. The presence of a simple peak diffraction at 2θ=20.88º relative to the sum of the diffractions at (1 1 0) and (2 0 0) planes, is

assigned to the electroactive β PVDF phase [25]. Similar results were obtained in the cooling process (**Figure 3b**).

Thermochromic response

During the experiments it was observed that the solution acquires a green color at room temperature during polymer dissolution. After spreading the solution in a glass substrate and heating up to 210 ºC, to guarantee polymer melting and solvent evaporation, the PVDF/$[Bmim]_2[NiCl_4]$ films show a color change from green to blue (**Figure 4a**). Finally, the films become transparent when the temperature decreases to room temperature. The color change is a reversible process and is temperature dependent. The color variations in the polymer films were quantitatively evaluated by UV-VIS spectroscopy at different temperatures between 30 and 70ºC, temperature range in which the color transition was observed. The UV-VIS curves for the different composites with different amounts of $[Bmim]_2[NiCl_4]$ are presented in **Figure 4b** and **4c**.

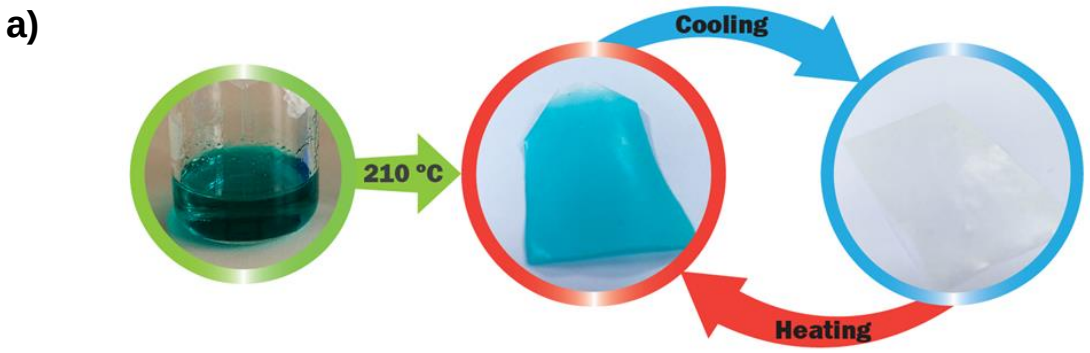

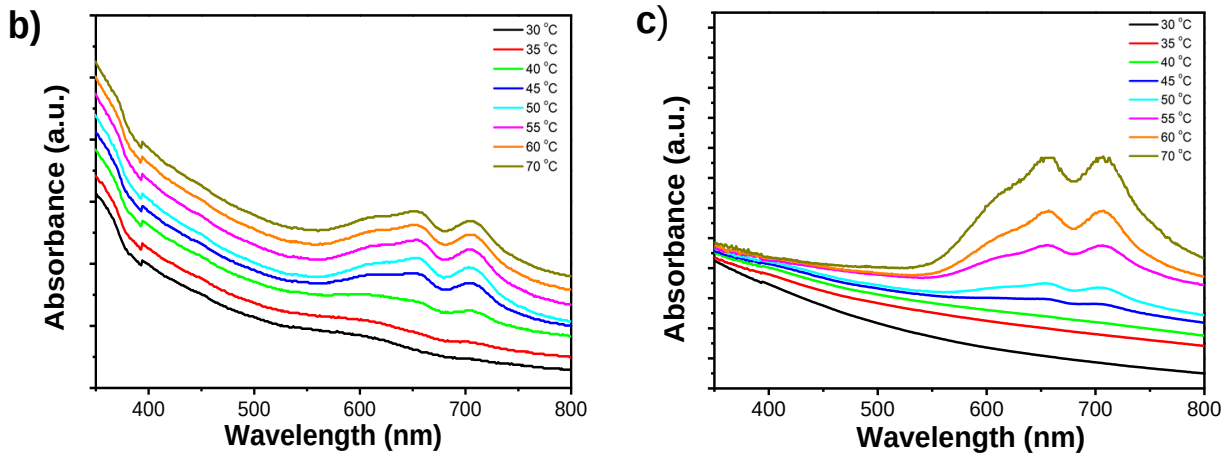

Figure 4. (a) Evolution of the color of the films with temperature variation for the PVDF/$[Bmim]_2[NiCl_4]$ film with 40 % wt. in IL. UV-VIS spectra of PVDF/$[Bmim]_2NiCl_4$ composites with different IL contents at various temperatures: 10 % wt. (b) and 40 % wt. (c).

Figure 4b and 4c show that the intensity in the blue region is highly dependent on the $[Bmim]_2[NiCl_4]$ content into the polymer matrix and increases with increasing temperature. A dark blue color is observed for the film with the incorporation of 40 % wt. into the polymer matrix (**Figure 4c**). It is also observed that the process is reversible, and the films recover transparency when temperature decreases back to room temperature. This reversible response can be visualized in **Figure 4a** and in the **supplementary information S2** video.

These results confirm the reversible thermochromism phenomena, characterized by a discontinuous effect in which the color change occurs more or less abruptly at a fairly distinct thermochromic color-change temperature corresponding to an abrupt change in the structure [9]. From the UV-VIS spectra of **Figure 4** it is observed strong variations in the absorption band in the peaks at 656 and 707 nm upon heating from 30 to 70 ºC. Both peaks show similar intensity, independently of the temperature, increasing the peak intensity with increasing temperature up to 70 ºC, which are attributed to the $[NiCl_4]^{2-}$ complex in its tetrahedral conformation (blue color) [11]. Moreover, with increasing $[Bmim]_2[NiCl_4]$ content from 10 to 40 % wt., an increase in the absorbance bands was observed, being the maximum absorption

reached at 60 and 70 ºC, respectively. The presence of only those absorption bands in the UV-VIS spectrum of the composites, independently of the $[Bmim]_2[NiCl_4]$ content, is an confirmation of the tetrahedral $[NiCl_4]^{2-}$ configuration as the only form in the films [11].

Thus, the color change of the films is explained by the modification of the coordination reaction. $[Bmim][NiCl_4]$ is a very hygroscopic salt, absorbing water molecules from the atmosphere. **Figure 5** shows the color evolution with increasing humidity (**Figure 5a**) and temperature (**Figure 5b**). With increasing humidity, no color changes were observed in the film, however, increasing temperature also leads to a decrease of the humidity, promoting the change of color to blue.

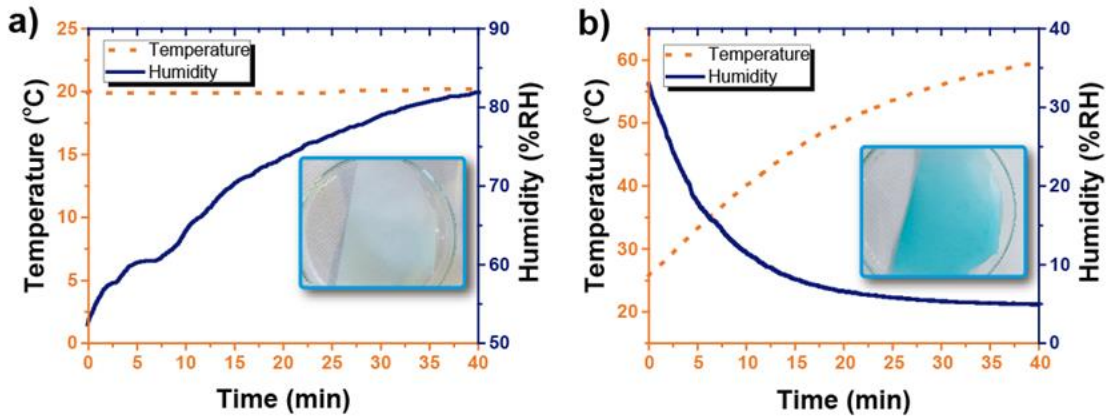

Figure 5. Effect of humidity at a constant temperature of 20 ºC (a) and effect of temperature (b) (with the increase of temperature there is a decrease in the humidity as well) on the color of the films.

In this sense, the observed thermochromism phenomena results from an thermally stimulated absorption/dehydration process, favored by the porous structure of the samples, which promotes changes in the coordination number of Ni(II) from octahedral to tetrahedral structure with no significant changes in the cation structure as shown in the **Scheme 1** below.

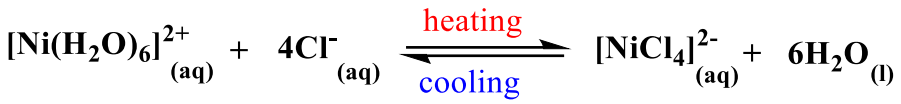

Scheme 1. Changes in the coordination number of Ni(II) from octahedral to tetrahedral structure.

At room temperature, and due to the hygroscopic nature of the IL, the water molecules in air replace the Cl^- ions into the nickel complex (octahedral structure) as a result of the H-bonding interactions with the anion $[NiCl_4]^{2-}$ in a symmetric complex (anion-H-O-H-anion). This leads to a disruption of the tetrahedral symmetry of blue colored $[NiCl_4]^{2-}$ [11, 37]. Upon heating at temperatures higher than 30 ºC, the water evaporation starts to occur as a result from a hydrothermochromic coordination reaction and the films change the color from transparent to dark blue (T>30 ºC) (**Figure 4**). As a result of the replacement of the water molecules by Cl^- atoms, the transition from an octahedral complex to a tetrahedral complex occurred (**Scheme 2**) [22, 37].

The cooling of the samples to room temperature leads to the inverse reaction, the films absorbing the atmospheric water and turning to its original transparent color.

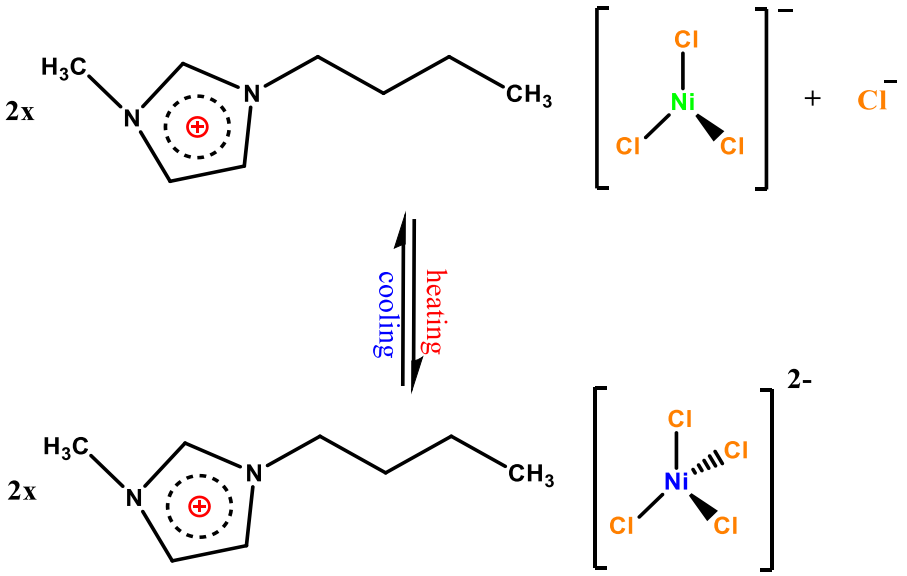

Scheme 2. Thermochromic chemical modifications that occur during heating and cooling.

Thermoresistive response

The conductivity of the samples was evaluated from the current vs voltage curves (inset of **Figure 6a**) and using **Equation 3. Figure 6a** presents the electrical conductivity of the composites as a function of the $[Bmim]_2[NiCl_4]$ content. It is observed a strong increase in the conductivity of the composites with increasing IL content. The conductivity of PVDF is around 5.0×10^{-12} S m^{-1} [34], increasing with IL content increase, with a stronger conductivity variation between 10-25 % of IL content. The maximum conductivity value was obtained for 40 % wt. of $[Bmim]_2[NiCl_4]$ (1.04×10^{-5} S m^{-1}) representing an increase of more than 6 orders of magnitude with respect to the value of PVDF.

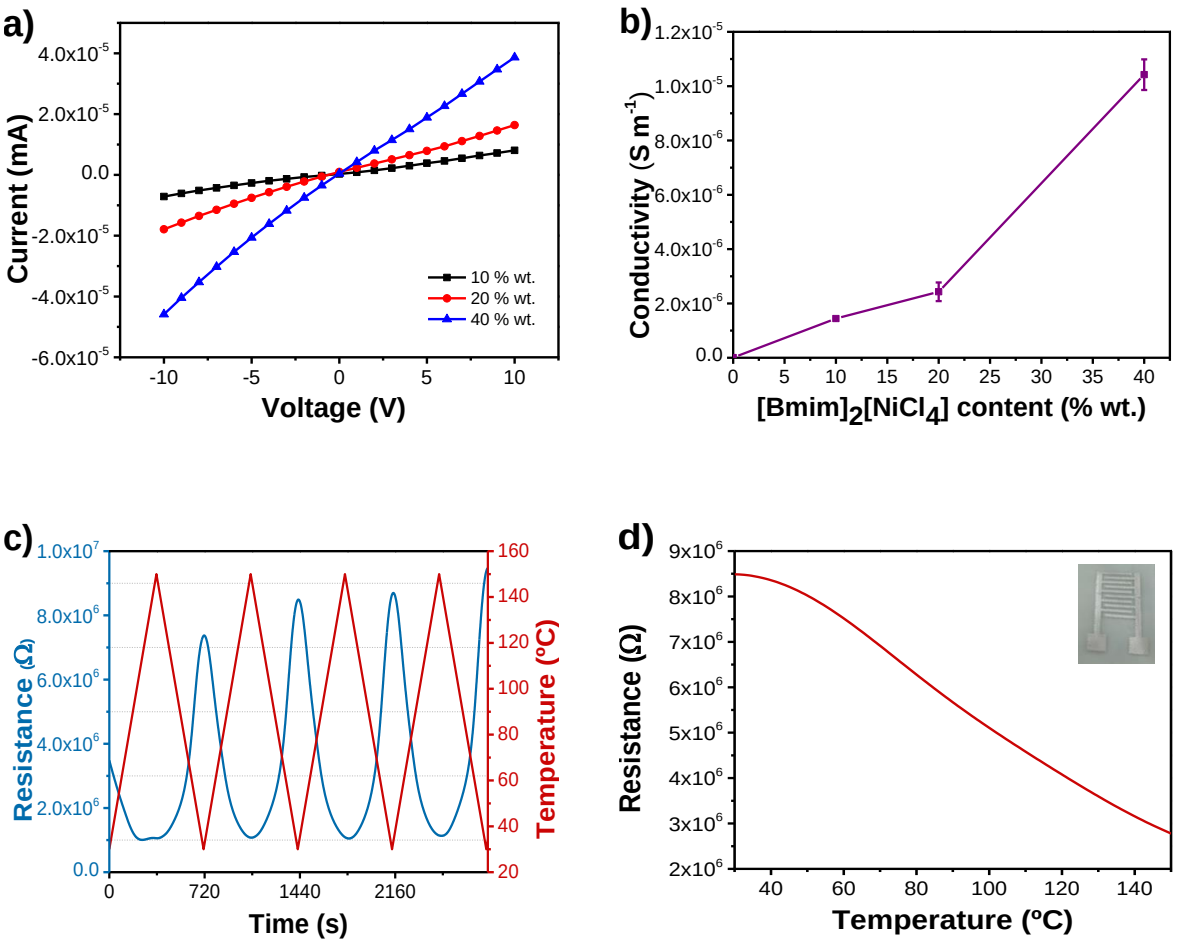

Figure 6. a) Current vs voltage curves, (b) electrical conductivity of the PVDF/IL composites as a function of $[Bmim]_2[NiCl_4]$ content, (c) Cyclic temperature dependence of the DC electrical conductivity between 30 and 150 °C for the composite containing 40 % wt. of $[Bmim]_2[NiCl_4]$ and (d) Resistance variation with the temperature.

The increase of the electrical conductivity within the composites results from the ionic properties of the ILs and ion-dipole interactions, being the ionic conductivity of the samples governed by the number and mobility of the cations and anions, viscosity and ionic charge of the IL [24]. The increase of the IL content into the polymer matrix promotes the dissociation and ions transport of the $[Bmim]_2[NiCl_4]$ leading to the increase of the number of carriers. This increase in the conductivity of the samples is also an indicative that the IL-polymer interaction among the polymer chain decrease as a result of IL content increase, promoting a fast dissociation of the ion transport from the polymer chain motion [24].

The effect of temperature variation as a function of time on the electrical resistance of the PVDF/$[Bmim]_2[NiCl_4]$ composites is presented in **Figure 6c and 6d**. The composites exhibiting a decrease in the electrical resistance with increasing temperature (increase of temperature upon heating) [41] and a good cyclability in terms of reversibility upon heating and cooling cycles, though the value of the overall resistance varies over cycling due to irreversible processes within the system. Independently of the amount of IL into the polymer matrix, the conductivity increases with increasing temperature, indicating that heating promotes a higher number of ion carrier. Furthermore, higher temperatures promotes the expansion of PVDF leading to expanded the free volume, which promotes increased mobility of both polymer segments and carrier ions [42]. It is to notice that during the heating, a dehydration process occurs and, therefore, the electrical conductivity can be ascribed to the IL ions and cations, as previously mentioned. In this sense, it is to notice that there are no specific anomalies in the thermal behavior of the electrical conductivity at temperatures in

which color variations are observed (**Figure 4**). Further, the electrical conductivity variation is nearly linear above 30 ºC, increasing with increasing temperature [43] and reversible upon hearing and cooling (**Figure 6c** and **6d**), showing the suitability of the PVDF/$[Bmim]_2[NiCl_4]$ composites for printable thermochromic and thermoresistive sensor applications, as it will be shown in the next section.

Printed thermochromic sensors

The developed PVDF/$[Bmim]_2[NiCl_4]$ composites can be applied for smart printable systems and sensors applications.

Adjusting the viscosity of the solution (1.08 Pa.s for a shear rate of 100 ($1.s^{-1}$)) [44], the developed solutions were adequate to smart printable systems, an area of an increasing interest (**Figure 6d** shows the thermoresistive sensor printed on interdigitated electrodes). These results are an indicative that the solution of PVDF/$[Bmim]_2[NiCl_4]$ can be applied as a smart ink, changing its color with varying temperature, as quantitatively shown in previous sections, finding applicability as a hot water level sensor (**Figure 7** and **supplementary video S3)** in which the optical properties of the material change with the temperature from transparent to blue (or vice versa) making them suitable as level sensors in the determination of the level of fluids. **Figure 7** shows a schematic representation of the water level sensor: when in contact with a vessel containing heated water, the film acquires a blue color indicative of the level of water. Obviously, a large range of applications can be pursued based on the aforementioned solution processable, i.e. printable, thermochromic and thermoresistive materials.

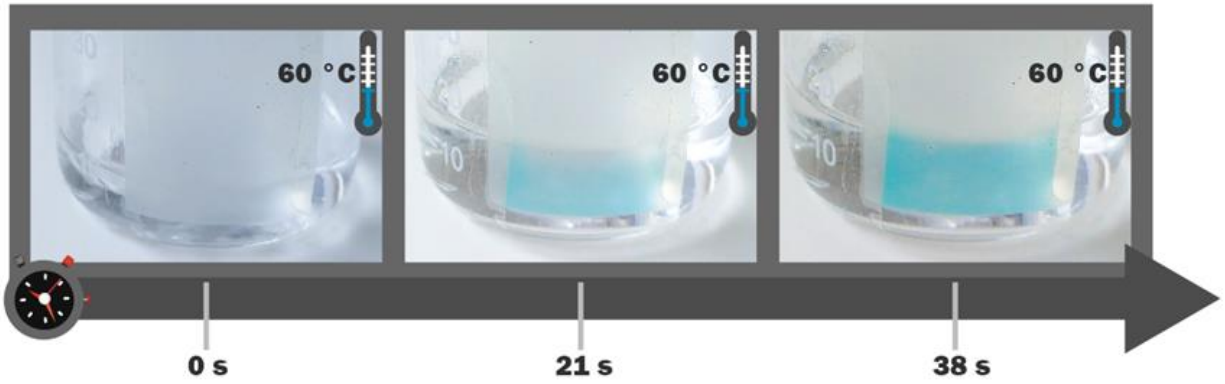

Figure 7. PVDF based $[Bmim]_2[NiCl_4]$ hot water level sensor based on PVDF/$[Bmim]_2[NiCl_4]$ composite containing 40 % wt. of IL.

Conclusions

PVDF based $[Bmim]_2[NiCl_4]$ solution processable, i.e. printable, thermochromic and thermoresistive films with different IL contents were obtained. The UV-VIS and X-ray analysis revealed that the reversible thermochromism behavior (transparent to blue or vice versa) results from a thermally induced dehydration process, which promotes changes in the coordination number of Ni(II) from octahedral to tetrahedral structure. Further, an increase in the electroactive β phase content of the PVDF polymer from 34 to 75 % is observed for the samples containing 20 % wt. of IL. The presence of the IL shows a minor effect on the degree of crystallinity of the polymer. Electrical measurements reveal an increase in the electrical conductivity with both increasing $[Bmim]_2[NiCl_4]$ content and temperature. These materials represent a promising solution for the development of thermochromic and thermoresistive printable sensors in areas such as temperature sensors, water level sensors or smart windows, among others.

Supporting Information

Supporting information S1 shows the SEM cross-section images of PVDF (a) and PVDF/$[Bmim]_2[NiCl4]$ with 10 % (b) wt, 20 % wt (c) and 40 % wt (d). Video S2 shows the variation of the optical properties of the material from transparent to blue (or vice versa) with varying temperature. Video S3 shows a hot water level sensor, based on the developed materials.

Corresponding authors:

Senentxu Lanceros-Mendez

Email: senentxu.lanceros@bcmaterials.net

Daniela Correia

Email: dcorreia@utad.pt

Acknowledgements

The authors thank the FCT - Fundação para a Ciência e Tecnologia - for financial support under framework of the Strategic Funding UID/FIS/04650/2013, the Associated Laboratory Research Unit for Green Chemistry, Technologies and Clean Processes, LAQV (financed by national funds from FCT/MEC, UID/QUI/50006/2013 and ERDF under the PT2020, POCI-01-0145-FEDER-007265) and project PTDC/EEI-SII/5582/2014 by FEDER funds through the COMPETE 2020 – Programa Operacional Competitividade e Internacionalização (POCI) with the reference project POCI-01-0145-FEDER-006941. Funds provided by FCT in the framework of EuroNanoMed 2016 call, Project LungChek ENMed/0049/2016 are also gratefully acknowledged. DMC, NP, and JMSSE also thank the grant/contract SFRH/BPD/121526/2016, SFRH/BD/131729/2017 and IF/00355/2012, respectively. The authors acknowledge funding by the Spanish Ministry of Economy and Competitiveness

(MINECO) through the project MAT2016-76039-C4-3-R (AEI/FEDER, UE) and from the Basque Government Industry and Education Departments under the ELKARTEK, HAZITEK and PIBA (PIBA-2018-06) programs, respectively.

References

(1) Costa, A. J. L.; Soromenho, M. R. C.; Shimizu, K.; Marrucho, I. M.; Esperança, J. M. S. S.; Lopes, J. N. C.; Rebelo, L. P. N. Density, Thermal Expansion and Viscosity of Cholinium-Derived Ionic Liquids. *ChemPhysChem* **2012,** *13* (7), 1902-1909, DOI: doi:10.1002/cphc.201100852.
(2) Lei, Z.; Chen, B.; Koo, Y.-M.; MacFarlane, D. R. Introduction: Ionic Liquids. *Chemical Reviews* **2017,** *117* (10), 6633-6635, DOI: 10.1021/acs.chemrev.7b00246.
(3) Wang, B.; Qin, L.; Mu, T.; Xue, Z.; Gao, G. Are Ionic Liquids Chemically Stable? *Chemical Reviews* **2017,** *117* (10), 7113-7131, DOI: 10.1021/acs.chemrev.6b00594.
(4) Dong, K.; Liu, X.; Dong, H.; Zhang, X.; Zhang, S. Multiscale Studies on Ionic Liquids. *Chemical Reviews* **2017,** *117* (10), 6636-6695, DOI: 10.1021/acs.chemrev.6b00776.
(5) Zhang, S.; Zhang, Q.; Zhang, Y.; Chen, Z.; Watanabe, M.; Deng, Y. Beyond Solvents and Electrolytes: Ionic Liquids-Based Advanced Functional Materials. *Progress in Materials Science* **2016,** *77*, 80-124, DOI: https://doi.org/10.1016/j.pmatsci.2015.10.001.
(6) Zhang, J.; Liu, H.; Jiang, L. Membrane-Based Strategy for Efficient Ionic Liquids/Water Separation Assisted by Superwettability. *Advanced Functional Materials* **2017,** *27* (20), 1606544, DOI: doi:10.1002/adfm.201606544.
(7) Guerrero-Sanchez, C.; Erdmenger, T.; Lara-Ceniceros, T.; Jimenez-Regalado, E.; Schuberta, U. S. Smart Materials Based on Ionic Liquids: the Magnetorheological Fluid Case. In *Ionic Liquids: From Knowledge to Application*; American Chemical Society: 2009; Chapter 10, pp 147-155.
(8) Drossel, W. G.; Meinel, F.; Bucht, A.; Kunze, H. Smart Materials for Smart Production – A Cross-Disciplinary Innovation Network in the field of Smart Materials. *Procedia Manufacturing* **2018,** *21*, 197-204, DOI: https://doi.org/10.1016/j.promfg.2018.02.111.
(9) Sone, K.; Fukuda, Y. Thermochromism of Transition Metal Complexes in the Solid State. In *Inorganic Thermochromism*; Springer Berlin Heidelberg: Berlin, Heidelberg, 1987; pp 104-131.
(10) Bloomquist, D. R.; Willett, R. D. Thermochromic Phase Transitions in Transition Metal Salts. *Coordination Chemistry Reviews* **1982,** *47* (1), 125-164, DOI: https://doi.org/10.1016/0010-8545(82)85012-1.
(11) Wei, X.; Yu, L.; Wang, D.; Jin, X.; Chen, G. Z. Thermo-Solvatochromism of Chloro-Nickel Complexes In 1-Hydroxyalkyl-3-Methyl-Imidazolium Cation Based Ionic Liquids. *Green Chemistry* **2008,** *10* (3), 296-305, DOI: 10.1039/B715763K.
(12) Yu, L.; Chen, G. Z. Cryo-Solvatochromism in Ionic Liquids. *RSC Advances* **2014,** *4* (76), 40281-40285, DOI: 10.1039/C4RA08116A.
(13) Perez, G.; Allegro, V. R.; Corroto, M.; Pons, A.; Guerrero, A. Smart Reversible Thermochromic Mortar for Improvement of Energy Efficiency in Buildings. *Construction and Building Materials* **2018,** *186*, 884-891, DOI: https://doi.org/10.1016/j.conbuildmat.2018.07.246.
(14) Cui, Y.; Ke, Y.; Liu, C.; Chen, Z.; Wang, N.; Zhang, L.; Zhou, Y.; Wang, S.; Gao, Y.; Long, Y. Thermochromic VO2 for Energy-Efficient Smart Windows. *Joule* **2018,** *2* (9), 1707-1746, DOI: https://doi.org/10.1016/j.joule.2018.06.018.
(15) Hao, L.; Ding, J.; Yuan, N.; Xu, J.; Zhou, X.; Dai, S.; Chen, B. Visual and Flexible Temperature Sensor Based on A Pectin-Xanthan Gum Blend Film. *Organic Electronics* **2018,** *59*, 243-246, DOI: https://doi.org/10.1016/j.orgel.2018.05.019.
(16) Warwick, M. E. A.; Binions, R. Chemical Vapour Deposition of Thermochromic Vanadium Dioxide Thin Films for Energy Efficient Glazing. *Journal of Solid State Chemistry* **2014,** *214*, 53-66, DOI: https://doi.org/10.1016/j.jssc.2013.10.040.

(17) Guan, Y.; Zhang, L.; Wang, D.; West, J. L.; Fu, S. Preparation of Thermochromic Liquid Crystal Microcapsules for Intelligent Functional Fiber. *Materials & Design* **2018,** *147*, 28-34, DOI: https://doi.org/10.1016/j.matdes.2018.03.030.
(18) Geng, X.; Li, W.; Wang, Y.; Lu, J.; Wang, J.; Wang, N.; Li, J.; Zhang, X. Reversible Thermochromic Microencapsulated Phase Change Materials for Thermal Energy Storage Application in Thermal Protective Clothing. *Applied Energy* **2018,** *217*, 281-294, DOI: https://doi.org/10.1016/j.apenergy.2018.02.150.
(19) Chen, H.-z.; Zhang, M.; Bhandari, B.; Yang, C.-h. Development of a Novel Colorimetric Food Package Label for Monitoring Lean Pork Freshness. *LWT* **2019,** *99*, 43-49, DOI: https://doi.org/10.1016/j.lwt.2018.09.048.
(20) Mejri, R.; Dias, J. C.; Hentati, S. B.; Martins, M. S.; Costa, C. M.; Lanceros-Mendez, S. Effect of Anion Type in The Performance of Ionic Liquid/Poly(Vinylidene Fluoride) Electromechanical Actuators. *Journal of Non-Crystalline Solids* **2016,** *453*, 8-15, DOI: https://doi.org/10.1016/j.jnoncrysol.2016.09.014.
(21) Gu, C.-D.; Tu, J.-P. Thermochromic Behavior of Chloro-Nickel(II) in Deep Eutectic Solvents and their Application in Thermochromic Composite Films. *RSC Advances* **2011,** *1* (7), 1220-1227, DOI: 10.1039/C1RA00345C.
(22) Wei, X.; Yu, L.; Jin, X.; Wang, D.; Chen, G. Z. Solar-thermochromism of Pseudocrystalline Nanodroplets of Ionic Liquid–NiII Complexes Immobilized inside Translucent Microporous PVDF Films. *Advanced Materials* **2009,** *21* (7), 776-780, DOI: doi:10.1002/adma.200801816.
(23) Mejri, R.; Dias, J. C.; Besbes Hentati, S.; Botelho, G.; Esperança, J. M. S. S.; Costa, C. M.; Lanceros- Mendez, S. Imidazolium-Based Ionic Liquid Type Dependence of The Bending Response of Polymer Actuators. *European Polymer Journal* **2016,** *85*, 445-451, DOI: https://doi.org/10.1016/j.eurpolymj.2016.10.052.
(24) Dias, J. C.; Martins, M. S.; Ribeiro, S.; Silva, M. M.; Esperança, J. M. S. S.; Ribeiro, C.; Botelho, G.; Costa, C. M.; Lanceros-Mendez, S. Electromechanical Actuators Based on Poly(Vinylidene Fluoride) with [N1 1 1 2(OH)][Ntf_2] and [C_2mim] [C_2SO_4]. *Journal of Materials Science* **2016,** *51* (20), 9490-9503, DOI: 10.1007/s10853-016-0193-0.
(25) Martins, P.; Lopes, A. C.; Lanceros-Mendez, S. Electroactive Phases of Poly(Vinylidene Fluoride): Determination, Processing and Applications. *Progress in Polymer Science* **2014,** *39* (4), 683-706, DOI: https://doi.org/10.1016/j.progpolymsci.2013.07.006.
(26) Mukai, K.; Asaka, K.; Kiyohara, K.; Sugino, T.; Takeuchi, I.; Fukushima, T.; Aida, T. High Performance Fully Plastic Actuator Based on Ionic-Liquid-Based Bucky Gel. *Electrochim. Acta* **2008,** *53* (17), 5555-5562, DOI: 10.1016/j.electacta.2008.02.113.
(27) Ferrari, S.; Quartarone, E.; Mustarelli, P.; Magistris, A.; Fagnoni, M.; Protti, S.; Gerbaldi, C.; Spinella, A. Lithium Ion Conducting PVdF-HFP Composite Gel Electrolytes based on N-methoxyethyl-N-methylpyrrolidinium Bis(trifluoromethanesulfonyl)-imide Ionic Liquid. *J. Power Sources* **2010,** *195* (2), 559-566, DOI: 10.1016/j.jpowsour.2009.08.015.
(28) Ye, H.; Huang, J.; Xu, J. J.; Khalfan, A.; Greenbaum, S. G. Li Ion Conducting Polymer Gel Electrolytes Based on Ionic Liquid/PVDF-HFP Blends. *J. Electrochem. Soc.* **2007,** *154* (11), A1048-A1057, DOI: 10.1149/1.2779962.
(29) Dias, J. C.; Correia, D. C.; Lopes, A. C.; Ribeiro, S.; Ribeiro, C.; Sencadas, V.; Botelho, G.; Esperanca, J.; Laza, J. M.; Vilas, J. L.; Leon, L. M.; Lanceros-Mendez, S. Development of Poly(Vinylidene Fluoride)/Ionic Liquid Electrospun Fibers for Tissue Engineering Applications. *Journal of Materials Science* **2016,** *51* (9), 4442-4450, DOI: 10.1007/s10853-016-9756-3.
(30) Wei, X.; Yu, L.; Jin, X.; Wang, D.; Chen, G. Z. Solar-thermochromism of Pseudocrystalline Nanodroplets of Ionic Liquid-Ni-II Complexes Immobilized inside Translucent Microporous PVDF Films. *Advanced Materials* **2009,** *21* (7), 776-+, DOI: 10.1002/adma.200801816.

(31) Zhong, C.; Sasaki, T.; Jimbo-Kobayeshi, A.; Fujiwara, E.; Kobayashi, A.; Tada, M.; Iwasawa, Y. Syntheses, Structures, and Properties of a Series of Metal Ion-containing Dialkylimidazolium Ionic Liquids. *Bulletin of the Chemical Society of Japan* **2007,** *80* (12), 2365-2374, DOI: 10.1246/bcsj.80.2365.
(32) Meredith, M. B.; McMillen, C. H.; Goodman, J. T.; Hanusa, T. P. Ambient Temperature Imidazolium-Based Ionic Liquids with Tetrachloronickelate(II) Anions. *Polyhedron* **2009,** *28* (12), 2355-2358, DOI: 10.1016/j.poly.2009.04.037.
(33) Nunes-Pereira, J.; Costa, C. M.; Leones, R.; Silva, M. M.; Lanceros-Mendez, S. Li-Ion Battery Separator Membranes Based on Poly(Vinylidene Fluoride-Trifluoroethylene)/Carbon Nanotube Composites. *Solid State Ionics* **2013,** *249*, 63-71, DOI: 10.1016/j.ssi.2013.07.021.
(34) Costa, P.; Nunes-Pereira, J.; Oliveira, J.; Silva, J.; Moreira, J. A.; Carabineiro, S. A. C.; Buijnsters, J. G.; Lanceros-Mendez, S. High-Performance Graphene-Based Carbon Nanofiller/Polymer Composites for Piezoresistive Sensor Applications. *Composites Science and Technology* **2017,** *153*, 241-252, DOI: https://doi.org/10.1016/j.compscitech.2017.11.001.
(35) Correia, D. M.; Martins, P.; Tariq, M.; Esperança, J. M. S. S.; Lanceros-Méndez, S. Low-Field Giant Magneto-Ionic Response in Polymer-Based Nanocomposites. *Nanoscale* **2018,** *10* (33), 15747-15754, DOI: 10.1039/c8nr03259a.
(36) Yassin, F. A.; El Kady, F. Y.; Ahmed, H. S.; Mohamed, L. K.; Shaban, S. A.; Elfadaly, A. K. Highly Effective Ionic Liquids for Biodiesel Production from Waste Vegetable Oils. *Egyptian Journal of Petroleum* **2015,** *24* (1), 103-11, DOI: 10.1016/j.ejpe.2015.02.011.
(37) Cammarata, L.; Kazarian, S. G.; Salter, P. A.; Welton, T. Molecular States of Water in Room Temperature Ionic Liquids. *Physical Chemistry Chemical Physics* **2001,** *3* (23), 5192-5200, DOI: 10.1039/b106900d.
(38) Dias, J. C.; Lopes, A. C.; Magalhães, B.; Botelho, G.; Silva, M. M.; Esperança, J. M. S. S.; Lanceros-Mendez, S. High Performance Electromechanical Actuators based on Ionic Liquid/Poly(Vinylidene Fluoride). *Polymer Testing* **2015,** *48*, 199-205, DOI: https://doi.org/10.1016/j.polymertesting.2015.10.012.
(39) Peixinho, J.; Lefèvre, G.; Coudert, F.-X.; Hurisse, O. Water Evaporation in Silica Colloidal Deposits. *Journal of Colloid and Interface Science* **2013,** *408*, 206-211, DOI: https://doi.org/10.1016/j.jcis.2013.07.013.
(40) Botelho, G.; Lanceros-Mendez, S.; Gonçalves, A. M.; Sencadas, V.; Rocha, J. G. Relationship Between Processing Conditions, Defects and Thermal Degradation of Poly(vinylidene fluoride) in the β-Phase. *Journal of Non-Crystalline Solids* **2008,** *354* (1), 72-78, DOI: https://doi.org/10.1016/j.jnoncrysol.2007.07.012.
(41) Horta-Romarís, L.; Abad, M.-J.; González-Rodríguez, M. V.; Lasagabáster, A.; Costa, P.; Lanceros-Méndez, S. Cyclic Temperature Dependence of Electrical Conductivity in Polyanilines as a Function of the Dopant and Synthesis Method. *Materials & Design* **2017,** *114*, 288-296, DOI: https://doi.org/10.1016/j.matdes.2016.11.021.
(42) Lopes, A. C.; Costa, C. M.; Serra, R. S. i.; Neves, I. C.; Ribelles, J. L. G.; Lanceros-Méndez, S. Dielectric Relaxation, Ac Conductivity and Electric Modulus in Poly(Vinylidene Fluoride)/Nay Zeolite Composites. *Solid State Ionics* **2013,** *235*, 42-50, DOI: https://doi.org/10.1016/j.ssi.2013.01.013.
(43) He, L.; Tjong, S.-C. Electrical Behavior and Positive Temperature Coefficient Effect of Graphene/Polyvinylidene Fluoride Composites Containing Silver Nanowires. *Nanoscale Research Letters* **2014,** *9* (1), 375, DOI: 10.1186/1556-276x-9-375.
(44) Oliveira, J.; Correia, V.; Castro, H.; Martins, P.; Lanceros-Mendez, S. Polymer-based Smart Materials by Printing Technologies: Improving Application and Integration. *Additive Manufacturing* **2018,** *21*, 269-283, DOI: https://doi.org/10.1016/j.addma.2018.03.012.

Table of Contents